Sorption time based sizing of a solid-state hydrogen storage bed and thermal management system

Chun-Sheng Wang and Joshua Brinkerhoff*,

School of Engineering, University of British Columbia, Kelowna, BC V1V 1V7, Canada

Abstract

Solid-state hydrogen (H_2) storage is a promising technology for transitioning to a carbon neutral H_2 economy. However, it is limited by the slow exothermic/endothermic reactions that occur during charging/discharging owing to the poor thermal conductivity of most solid-state H_2 storage materials. Although many researchers have addressed this challenge using various thermal management systems (TMSs), there is a lack of design tools available for sizing the reaction bed and TMS. This study aims to develop a multi-level model to size the solid-state storage system consisting of the reactor and the corresponding TMS. The sizing models are based on the sorption-time, an indicator that is crucial to the solid-state H_2 storage technology. In addition, the proposed sizing procedure contains an inner loop and outer loop that apply the algebraic model (AM) and a combined lumped parameter model/computational fluid dynamics (LPM/CFD) model, respectively, resulting in marked reduction in solution time. Validations are conducted through comparison of AM predicted results with those of the experiments on solid-state H_2 storage involving both internal and external TMSs. As the computational cost for the AM is negligible, the developed multi-level model facilitates the sizing of industrial-scale solid-state H_2 storage systems with large or complex reactor beds and sophisticated TMSs.

Keywords: Solid-state hydrogen storage, Sorption time, Sizing model, Metal hydrides, Thermal management

1. Introduction

Hydrogen (H_2) storage using solid-state materials is an emerging technology that contributes to carbon neutrality [1-3]. It can be applied in numerous industries such as transportation, metal refining, power generation, and indoor heating/refrigeration, etc. The solid-state materials are mainly classified into two groups: chemisorptive (e.g. metal hydrides) and physisorptive (e.g. activated carbon) [4, 5]. The chemisorptive materials store H_2 via reversible chemical bond whereas the physisorptive ones rely on Van der Waals forces. For most solid-state H_2 storage materials, the adsorption and desorption process are respectively exothermic and endothermic with sorption heat in the range of 1-10 kJ/mol H_2 for physisorption and 20-80 kJ/mol H_2 for chemisorption [2, 6]. The reaction heat markedly affects the kinetics and increases the H_2 charging/discharging duration [2, 6, 7], which is unfavorable for applications demanding short charging or discharging periods (e.g. H_2 fuel cell electric vehicles).

To address this challenge, the design of solid-state H_2 storage tanks with highly efficient thermal management systems (TMSs) is required [2, 6, 7]. In general, TMSs fall into two broad categories: internal and external. Internal TMSs bring a liquid coolant into the tank while external ones circulate the coolant around the tank outer wall. For the external TMS, Jemni et al. [7] experimentally and numerically explored the mass and heat transfer during H_2 adsorption and desorption in a $LaNi_5$ cylinder chamber submerged in a bath. They showed the poor thermal conductivity of the porous $LaNi_5$ bed. Muthukumar et al. [8] measured the mass and heat transfer in an annular $MmNi_{4.6}Fe_{0.4}$/$MmNi_{4.6}Al_{0.4}$ storage bed with an external water jacket during the adsorption process using experimental techniques. Muthukumar et al. [8] concluded that the adsorption duration decreases with increasing initial pressure and enhanced heat transfer in the tank. Phate et al. [9] studied the effects of aspect ratio and hydride porosity in a cylindrical tank filled with $LaNi_5$ using 2D computational fluid dynamics (CFD) simulations. The external thermal management was the same as Jemni et al. [7]. It was found that the saturation (adsorption) time increases with both aspect ratio and porosity.

* Corresponding author.
Email address: joshua.brinkerhoff@ubc.ca (J. Brinkerhoff).

Nomenclature

AR	Aspect ratio
c_p	Specific heat capacity ($\mathrm{J/kg \cdot K}$)
C_b	Storage bed thermal capacity (J/K)
C_{wt}	Gravimetric H_2 capacity
D_{tank}	Tank outer diameter (m)
h	Heat transfer coefficient ($\mathrm{W/m^2 \cdot K}$)
k_e	Effective or mean thermal conductivity of porous bed ($\mathrm{W/m \cdot K}$)
k_f	Thermal conductivity of H_2 gas ($\mathrm{W/m \cdot K}$)
k_{tank}	Thermal conductivity of tank wall ($\mathrm{W/m \cdot K}$)
K	Permeability ($\mathrm{m^2}$)
L	Characteristic length (m)
m_g	Total mass of hydrogen gas
$\dot{m}$	Hydrogen sorption rate (kg/s)
Pr	Prandtl number, $Pr = \nu/\alpha_m$
$\dot{q}$	Sorption heat flux (W)
r, y	Cylindrical coordinates (m)
R	Sorption bed radius (m)
R_b	Tank inner radius (m)
R_{bed}	Bed thermal resistance (K/W)
R_g	Specific gas constant ($\mathrm{J/kg \cdot K}$)
t	Time (s)
t_s	Sorption time (s)
T	Temperature (K)

Greek symbols

α_m	Mean or effective thermal diffusion coefficient ($\mathrm{m^2/s}$)
β	Thermal expansion coefficient ($1/\mathrm{K}$)
Δt	Time step (s)
ε	Porosity
ν	Kinematic viscosity ($\mathrm{m^2/s}$)
ρ	Density ($\mathrm{kg/m^3}$)
ρ_g	Density of hydrogen ($\mathrm{kg/m^3}$)
ρ_s	Density of storage material ($\mathrm{kg/m^3}$)
σ	Heat capacity ratio

Subscripts

bed	Storage bed
fin	Fins
g	Hydrogen gas
i, o	Inner and outer radius
m	Mean
s	Storage material
tank	Storage tank

Yang et al. [10, 11] numerically analyzed three externally cooled beds on the sorption time of a $LaNi_5$ reactor. It was spotted that the annulus bed configuration exhibits the shortest charging time. Nam et al. [12] performed parametric study of H_2 adsorption in a $LaNi_5$ reactor with an external cooling system using 3D CFD simulations. The effect of H_2 fraction on the equilibrium pressure was found to be significant during the charging process. Moreover, the external surface to volume ratio of the chamber markedly affected the charging duration. Mellouli et al. [13] simulated spherical and cylindrical Mg reactors cooled or heated by a phase change material (PCM) surrounding the reactor's outer surface. The adsorption/desorption time of the spherical reactor was higher than the cylindrical reactor. Lin et al. [14] studied the volumetric expansion, particle radius and porosity on the H_2 adsorption time in a $LaNi_5$ bed with external cooling using CFD, for which they noted that adsorption time increases with increasing the particle radius or decreasing porosity. Manai et al. [15] numerically explored the influences of different bed configurations on H_2 charging in a $Ti_{0.95}Zr_{0.05}Mn_{1.48}Fe_{0.08}Al_{0.01}$ reactor with external cooling. They concluded that the best heat transfer is achieved for the compact bed configuration with alternate metal hydride and gas layers. Afzal and Sharma [16] simulated the H_2 adsorption in a $La_{0.9}Ce_{0.1}Ni_5$ bed with internal hexagonal honeycomb shaped fins. Compared with the smooth case, the finned reactor charged 30% faster. Afzal et al. [17] subsequently conducted experiments on the performance of hexagonal honeycomb-shaped fins, finding that the finned tank with evaporative cooling reduced the charging time by 57%.

For internal TMSs, Hardy and Anton [18, 19] numerically researched a $NaAlH_4$ ($TiCl_3$ catalyzed) reactor with and without internal fins. They concluded that the reaction bed with internal fins quickly removes the sorption heat and in turn leads to reduced adsorption time. Askri et al. [20] applied concentric tubes and fins to shorten the adsorption time of a $LaNi_5$ reactor by numerical simulations. In comparison to the cylindrical chamber, the annulus bed configuration with internal fins reduces the charging duration by 80%. Bao et al. [21] adopted numerical simulations to explore the heat and mass transfer in Mg storage tanks. The best operating condition for minimizing the H_2 charging time was spotted. Singh et al. [22] proposed internal conical fins to reduce the adsorption time of a $LaNi_5$ reaction bed to via 3D simulations. The conical fins were found to decrease the charging duration (defined as the time to reach 90% H_2 saturation) by 75% relative to the reference case. Kumar et al. [23] experimentally investigated H_2 sorption inside a $MmNi_{4.7}Fe_{0.3}$ bed with internal coolant tubes.

A few optimized parameters such as the coolant flow rate and H_2 supply pressure and temperature are proposed for mobile and stationary H_2 storage applications. Eisapour et al. [24] conducted numerical optimization of heat transfer in a cylinder Mg_2Ni-H_2 bed with helical coil coolant channels. By optimizing the tube diameter, coil diameter and pitch, the adsorption time was 24% lower than that of the baseline case without a central tube. Bai et al. [25] proposed novel tree-shaped fins for the cooling of a cylinder $LaNi_5$ reactor during the H_2 adsorption. In comparison with the basic radial fins, the tree-shaped fins achieved a 20.7% lower adsorption time.

Tandem internal and external TMS have also been studied. Kikkinides et al. [26] numerically simulated combining external and internal cooling on the sorption performance of $LaNi_5$ storage devices. They demonstrated that the adsorption/desorption times are shortened by 60% with an optimized reactor cooling and operating strategy. Mellouli et al. [27] numerically explored the fin length, thickness, and configuration on H_2 charging of a $LaNi_5$ reactor with an external water jacket and internal cooling tubes. Charging time reductions of up to 66% of the reference case were obtained. Similarly, Karmakar et al. [28] measured the sorption performance of a 10 kg $LaNi_5$ reactor with internal coolant tubes and external forced water cooling, achieving a 46% percent reduction in adsorption time at a gravimetric capacity of 1.13 wt%.

The above studies primarily focus on experimental or CFD studies on enhancing the heat transfer in H_2 storage systems during charging or discharging with the aim of reducing the sorption time. There are few studies addressing sizing of the reaction bed and TMS for a target sorption time. Such design sizing generally occurs in an iterative fashion and may require a large number of design iterations. Since the computational cost of CFD simulation (in terms of simulation times, memory and file storage requirements, and computational hardware) are relatively high [29, 30], especially for large industrial H_2 storage systems, it is infeasible to develop a sizing design tool based on CFD simulations only. To resolve this issue, we aim to develop a multi-level framework that can quickly and accurately size solid-state H_2 storage reactor beds and TMSs for a target sorption time.

2. Overview of solid-state hydrogen storage system and its modelling

A general concept of the H_2 storage system using solid-state chemisorptive/physisorptive materials are illustrated in Fig. 1. The H_2 storage system is comprised of a single tank or an array of tanks [31] and the corresponding TMS. H_2 enters or leaves the storage vessel for refueling from a H_2 station or end-use appliance, respectively. The solid-state storage material is in the form of a powder and considered as porous media with low thermal conductivity. During the charging or discharging process, the sorption heat is managed by the TMS that rejects/draws heat to/from the heat sink/source through either thermal radiation, convection, or conduction. As detailed above, the mass transport of H_2 during the charging/discharging process is strongly dependent on the corresponding heat transfer. In turn, the sorption heat generated during H_2 transport also influences the heat transfer. In other words, the two transport processes are coupled. Since the time required for the adsorption process is more critical in practical applications, the sizing of the storage system will be based on the H_2 charging. To size the system, we assume that the total mass of H_2 (m_g) and storage material as well as its operating pressure and temperature (thus, the gravimetric H_2 capacity C_{wt}) are given, and our goal is to find a design that meets the target charging time (t_s) and optimizes the effective H_2 gravimetric capacity ($C_{wt,e}$) or cost. Here, the gravimetric H_2 capacity C_{wt} is generally defined by

$$C_{wt} = \frac{m_g}{m_g + m_{s,tot}}, \tag{1}$$

where $m_{s,tot}$ is the total mass of the solid storage material. Similar to C_{wt}, $C_{wt,e}$ for the whole storage system is defined as

$$C_{wt,e} = \frac{m_g}{m_g + m_{s,tot} + m_{sys}}. \tag{2}$$

Here, m_{sys} denotes the mass of the empty tanks and non-detachable parts of the TMS such as the fins, cooling tubes, etc. The sorption time t_s is defined as [22]

$$t_s = t|_{\phi_H=90\%}, \tag{3}$$

where ϕ_H is the reacted fraction of H_2. Note that ϕ_H versus t is an asymptotic curve and the theoretical charging time is infinity at $\phi_H = 100\%$. Thus, the above definition for the charging time is applied. Some literature [17,

32] also uses the time at $\phi_H = 80\%$ or 95% as the charging time. According to Eq. (2) and Eq. (3), if the required t_s is short, sophisticated TMSs must be applied, which may result in larger m_{sys} and decreased $C_{wt,e}$ and increased cost. Thus, for a specific t_s, there must exist an optimal design for maximal $C_{wt,e}$ and/or minimal cost.

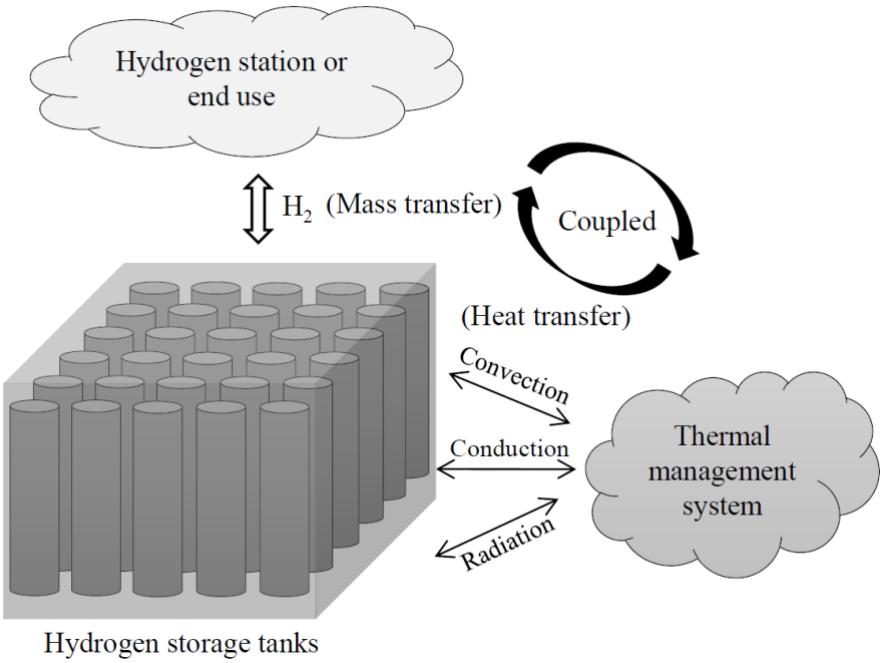

Fig. 1 Solid-state hydrogen storage system that consists of storage tanks and TMS.

Fig. 2 shows a single H_2 storage tank of the tank array in Fig. 1 with an internal or external TMS for the adsorption process. Here, we assume that the tank geometry and the cooling system are identical for each tank in the storage vessel. The TMS for solid-state H_2 storage may be internal or/and external. The internal cooling technique generally applies internal fins and cooling tubes to reject the heat to the coolant in the while the external one relies on the internal and/or external fins to dissipate the heat to the ambient fluid. The corresponding heat transfer mechanism could be heat conduction, heat convection, or thermal radiation.

Modelling the mass (H_2) and heat transport in the storage system can be performed in at least three different ways, summarized in Table 1: solving the integral form of mass and energy conservation equation with respect to time and space, solving the integral form of mass and energy conservation equation with respect to space only, and solving the differential form of mass, momentum, and energy conservation equation (namely the Navier-Stokes-Fourier equations). These modelling approaches respectively yield a system of algebraic equations, ordinary differential equations (ODEs), and partial differential equations (PDEs), which are respectively called algebraic model (AM), lumped parameter model (LPM) (or thermal resistance network) [30], and computational fluid dynamics (CFD) model [18,19, 29]. Due to the different levels of simplification, the accuracy as well as the computational cost is quite different. The computational cost and accuracy are always contradictory in computational science. In general, the AM has the lowest computational cost but also poorest accuracy while the CFD is the opposite. Although the accuracy of AM is not always satisfactory, it could be used to generate initial designs for further LPM/CFD optimization to reduce the number of design iterations during sizing due to the negligible computational cost. Therefore, a multi-level model will be proposed in this study to size the H_2 storage system, with a focus on the AM since the LPM and CFD have been addressed in our previous publications [29, 30].

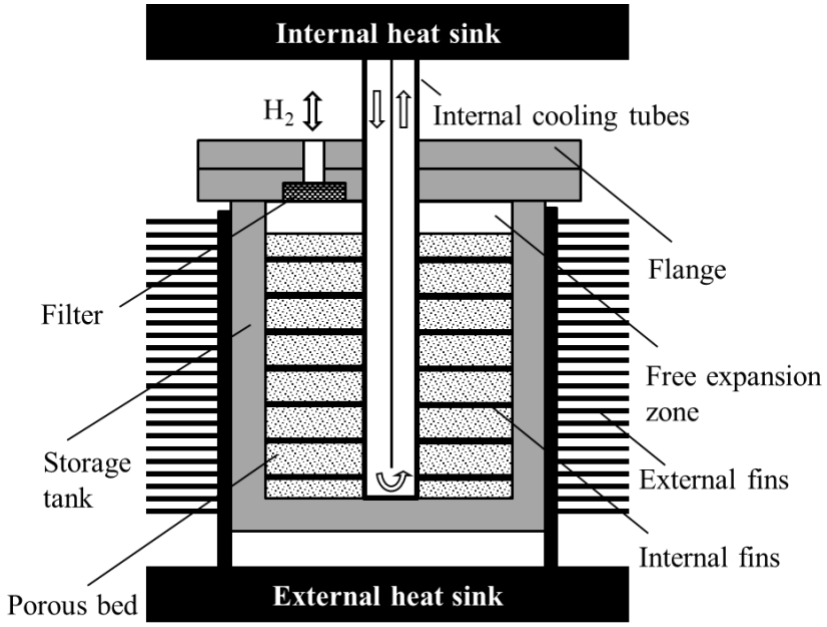

Fig. 2 Schematic diagram of a general solid-state H_2 storage tank with internal or external TMS.

Table 1 Comparison of three levels of models for predicting the heat and mass transfer in a solid-state hydrogen storage system.

Model	Governing Equations	Equation Type	Accuracy	Computational Cost
AM	Integral form of mass and energy conservation equation with respect to time and space	Algebraic	Low	Negligible
LPM	Integral form of mass and energy conservation equation with respect to space only	ODEs	Moderate	Low
CFD	Differential form of mass, momentum, and energy conservation equation (Navier-Stokes-Fourier equations)	PDEs	High	High

In our previous work [33], a general time scale was proposed to estimate the charging time for solid-state materials, which reads

$$t_{TD} = \sigma L^2/\alpha_m = \frac{L^2}{k_e/(\rho c_p)_e}. \quad (4)$$

However, the sorption time model considers only the porous media bed (without internal fins and TMS). To find out a generalized algebraic expression for both the sorption bed and TMS, we will need to look at the differential equation. Fig. 3 shows the transient thermal resistance network of the storage system in LPM modeling. For either internal or external cooling, the differential energy equation can be written in a consistent form as

$$\dot{q} = C_{bed}\frac{dT_{bed}}{dt} + \frac{T_{bed} - T_a}{R_{tot}}, \tag{5}$$

where $\dot{q} = \dot{m}\left[\Delta H + T\left(c_{p,g} - c_{p,s}\right)\right]$ and R_{tot} denotes the total thermal resistance of the bed and TMS. There does not exist an explicit solution for the above equation since the heat and mass transfer are coupled. To find out an approximate solution, we assume that the cooling phase of the adsorption process in which sorption heat is transferred through the storage system takes much longer than the heating phase during which the sorption heat is produced. This means that the heat generation term is neglected. Without the heat generation term, the thermal resistance network becomes a RC circuit and an explicit solution can be obtained as

$$\frac{T_{bed} - T_a}{T_{bed,max} - T_a} = \exp\left(-\frac{t}{C_{bed}R_{tot}}\right). \tag{6}$$

If t_s is defined at $(T_{bed} - T_a)/\left(T_{bed,max} - T_a\right) = 5\%$, we have

$$t_s = R_{tot}C_{bed}\ln(20) = 3R_{tot}C_{bed}. \tag{7}$$

For a pure cylindrical porous media bed, $C_{bed} = V_s\left(\rho c_p\right)_e = \pi R^2 H\left(\rho c_p\right)_e$ and $R_{tot} \approx R_{bed} = ln(R/R_e)/(2\pi H k_e) = ln(2)/(2\pi H k_e)$. In such conditions, t_s is given by

$$t_s = 3R_{tot}C_{bed} = 3\frac{ln(2)}{(2\pi H k_e)}\pi R^2 H\left(\rho c_p\right)_e = \frac{1.04R^2}{k_e/\left(\rho c_p\right)_e}. \tag{8}$$

Obviously, the above equation is very close to Eq. (4) ($L = R$ for cylindrical beds). Thus, Eq. (7) can be used as a general expression for estimating t_s. Also, from Eq. (7) it is seen that t_s is proportional to the total thermal resistance, meaning that if the thermal resistance of the TMS is much smaller than that of the bed, further improvements of the TMS (e.g., increased coolant volume rate in the internal or external cooling system) will no longer contribute to reducing the sorption time. This aligns with previous experimental results [8, 34]. In this scenario, we must decrease the effective thermal resistance of the porous bed (e.g., using internal fins) to further reduce the sorption time.

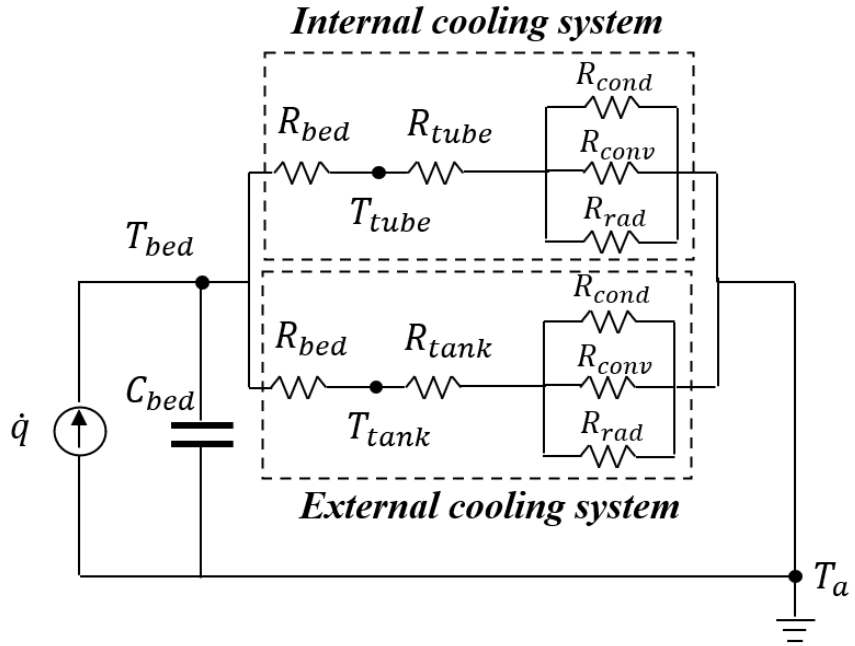

Fig. 3 LPM modelling of the solid-state hydrogen storage system using thermal resistance network.

3. Sizing of storage tanks

In this section, we will derive the AM for sizing the storage tank based on the generalized sorption time model. Note that the tank size here refers to the inner tank size excluding the thickness of tank wall. Fig. 4 shows the porous media sorption bed with internal fins, cooling tubes, free expansion region, and passage for H_2 flow. As a general case, we assume the number of tanks (N_{tank}) exceeds one. According to Eq. (1), the total mass of the storage material is calculated as

$$m_{s,tot} = m_g\left(\frac{1}{C_{wt}} - 1\right) = N_{tank}\rho_s V_s(1-\varepsilon), \tag{9}$$

where ε is the bed porosity and V_s is the volume of the storage material.

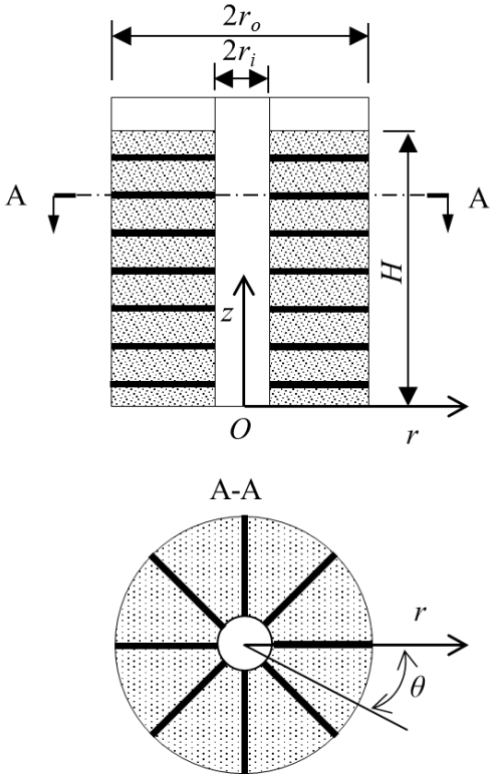

Fig. 4 Sorption bed with internal fins and cooling tubes.

The total volume of the storage tank can be expressed as

$$V_{tank} = \pi R^2 H = \pi R^3 AR = V_s\left(1 + C_{ve} + C_{vf} + C_{vt} + C_{vo}\right), \tag{10}$$

where $C_{ve} = V_{expand}/V_s$, $C_{vf} = V_{fin}/V_s$, $C_{vt} = V_{tube}/V_s$, $C_{vo} = V_{other}/V_s$, and $AR = H/R$.

For Eq. (8), if the thermal resistance of the TMS is much smaller than that of the bed, we have

$$t_s = 3R_{bed}V_s\left[\left(\rho c_p\right)_e + C_{vf}\left(\rho c_p\right)_{fin}\right] \tag{11}$$

The thermal resistance of the bed can be estimated as

$$R_{bed} = \eta_c\frac{L}{k_e A} = \eta_c\frac{(1-C_R)}{2\pi AR k_e R} \tag{12}$$

where $r_o = R$, $r_i = RC_R$, and η_c is the fin or cooling tube performance factor that ranges from 0 to 1. η_c varies with internal fin/cooling tube arrangement and adsorption equilibrium pressure/temperature. From the previous literature [7, 8, 28, 31, 34, 35], η_c is found as a function of C_{vf} for a fixed equilibrium pressure and temperature as shown in Fig. 5. Through curve fitting, $\eta_c = (1 - 1.4C_{vf})^{0.769}$. Generally, η_c can be estimated as $\eta_c = L_{bed}/[R(1 - C_R)]$, where L_{bed} is the maximum distance between any point in the porous and the nearest fins or tank walls. Substituting Eq. (12) into Eq. (11), we have

$$t_s = \frac{3\eta_c(1 - C_R)V_s}{2\pi AR k_e R}\left[\left(\rho c_p\right)_e + C_{vf}\left(\rho c_p\right)_{fin}\right] \tag{13}$$

Combine Eq. (13) and (10), R and AR are respectively solved as

$$R = \sqrt{\frac{2k_e t_s\left(1 + C_{ve} + C_{vf} + C_{vt} + C_{vo}\right)}{3\eta_c(1 - C_R)\left[\left(\rho c_p\right)_e + C_{vf}\left(\rho c_p\right)_{fin}\right]}}, \tag{14}$$

$$AR = \frac{\left(\frac{1}{C_{wt}} - 1\right) m_g \left\{3\eta_c(1 - C_R)\left[\left(\rho c_p\right)_e + C_{vf}\left(\rho c_p\right)_{fin}\right]\right\}^{3/2}}{\pi N_{tank}\rho_s(1 - \varepsilon)(4k_e t_s)^{3/2}\sqrt{\left(1 + C_{ve} + C_{vf} + C_{vt} + C_{vo}\right)}}. \tag{15}$$

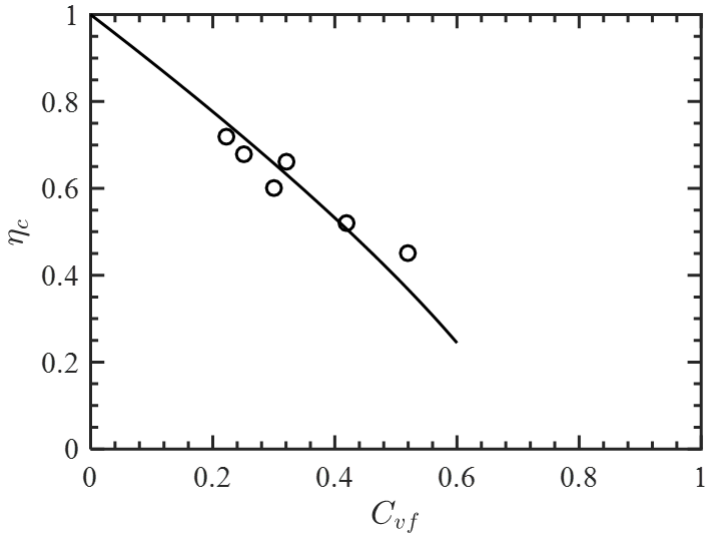

Fig. 5 η_c as a function of C_{vf} evaluated from the previous experimental data.

4. Sizing of thermal management system

As mentioned above, liquid cooling for application to the sorption bed is generally divided into the two main categories of internal and external liquid cooling. Internal liquid cooling brings the liquid coolant into the tank (Fig. 2), while in external liquid cooling, the liquid does enter the storage tank (Fig. 2). Generally, internal cooling methods have less conduction thermal resistance compared to that of external cooling since the cooling tubes are in direct contact with the porous bed. However, due to the relatively high pressure inside the tank, there may be the risk of coolant leakage into the storage material.

For either TMS, the total heat that needs to be rejected is given by the following equation according to energy conservation,

$$Q_{tot} = m_g \Delta H + \int \dot{m} T \left(c_{p,g} - c_{p,s}\right) \approx m_g \left[\Delta H + T_a \left(c_{p,g} - c_{p,s}\right)\right]. \tag{16}$$

For a given sorption time t_s, the average heat flux for each tank is determined as

$$\dot{q}_{avg} = \frac{Q_{tot}}{N_{tank} t_s} = \frac{m_g \left[\Delta H + T_a \left(c_{p,g} - c_{p,s}\right)\right]}{N_{tank} t_s}, \tag{17}$$

where ΔH denotes the sorption heat for the storage material. For the heat sink, the cooling heat load is given by

$$\dot{q}_{avg} = \frac{T_{bed,avg} - T_a}{\frac{1}{h_{avg} A_{surf}} + R_{bed}}. \tag{18}$$

Here, we define the cooling surface area $A_{surf} = C_{As} 2\pi RH = C_{As} 2\pi R^2 AR$. Thus, the required surface heat transfer coefficient h_{avg} is estimated as

$$h_{avg} = \left\{ 2\pi R^2 AR C_{As} \left[\frac{t_s N_{tank} (T_{bed,avg} - T_0)}{m_g \left(\Delta H + T_a \left(c_{p,g} - c_{p,s}\right) \right)} - R_{bed} \right] \right\}^{-1}, \tag{19}$$

where $T_{bed,avg} - T_0 = 0.25 \left[\Delta H + T_a \left(c_{p,g} - c_{p,s}\right)\right] m_g / \left[V_s \left(\rho c_p\right)_e\right]$. Note that h_{avg} is the total surface heat transfer coefficient from the three heat transfer mechanisms mentioned above. If the thermal resistance of the TMS is much smaller than that of the bed ($R_{th} \leq 0.1 R_{bed}$), we also have

$$R_{th} = \frac{1}{h_{avg} A_{surf}} \leq 0.1 \eta_c \frac{0.5(1 - C_R)}{2\pi AR k_e R}. \tag{20}$$

If h_{avg} is fixed for a selected cooling system, the surface area ratio C_{As} should satisfy

$$C_{As} \geq \frac{20 k_e}{\eta_c (1 - C_R) R h_{avg}}. \tag{21}$$

The problem involves using more cooling tubes for the internal cooling system or extension of the effective tank surface area using external fins for the external cooling system. If A_{surf} is fixed, h_{avg} should meet the requirement:

$$h_{avg} \geq \frac{2\pi AR k_e R}{0.05 \eta_c (1 - C_R) A_{surf}} = \frac{20 k_e}{\eta_c (1 - C_R) R C_{As}}. \tag{22}$$

The problem reduces to the selection of cooling techniques. According to the estimated value of h_{avg}, appropriate cooling techniques may be chosen.

The achievable surface heat transfer coefficient for different cooling technology is shown in Fig. 6 [36]. The typical coolant fluid includes the air, water, and water-glycol (WG) mixture. Although the WG mixture shows poorer thermal conductivity than that of the water, the working temperature may go below -30 °C. In addition, the cooling techniques with larger h_{avg} generally have higher costs but also better compactness (namely larger $C_{wt,e}$) according to Eq. (21). Thus, a tradeoff between cost and $C_{wt,e}$ should be considered. Table 2 shows the cooling techniques used in the previous experiments for solid-state H_2 storage. It is observed that the corresponding h_{avg} is within the range in Fig. 6.

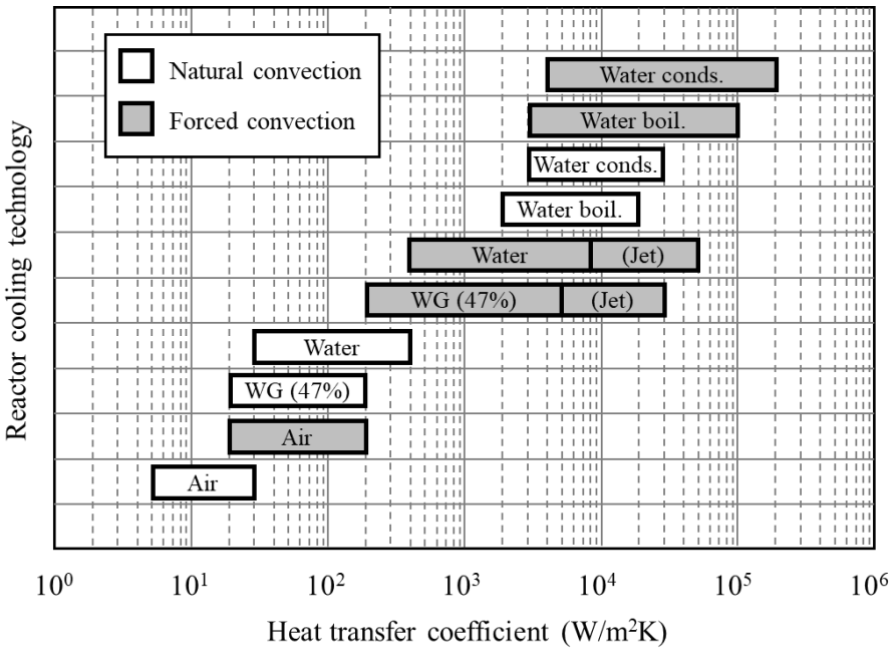

Fig. 6 Heat transfer coefficient range for different cooling technologies.

Table 2 Summary of the cooling techniques used in the previous experiments for solid-state H_2 storage.

Author and year	Storage material	Tank no.	TMS category	Cooling technologies	h_{avg} (W/m^{2}K)	Fins
Jemni et al., 1999 [7]	$LaNi_5$	1	External	Forced convection with water	1625	NA
Muthukumar et al., 2005 [8]	$MmNi_{4.6}Fe_{0.4}$ $MmNi_{4.6}Al_{0.4}$	1	External	Forced convection with water	750-1250	Internal & external
Chaise et al., 2010 [35]	Mg	1	Internal	Forced convection with air	NA	Internal
Garrier et al., 2011 [34]	Mg	1	Internal	Forced convection with air	1040	Internal
Lototskyy et al., 2020 [31]	C14-AB2 Laves-type alloy	5	External	Forced convection with water	NA	External
Karmakar et al., 2021 [28]	$LaNi_5$	1	Internal & External	Forced convection with water	NA	Internal
Kumar et al., 2021 [23]	$MmNi_{4.7}Fe_{0.3}$	1	Internal	Forced convection with water	1610-2140	NA

4.1. Internal TMS

For a typical internal TMS in Fig. 7, considering the relatively small C_{As} ($C_{As} < 1$), higher values of h_{avg} are desired. Thus, the forced convection of air or water is generally used. In addition, phase-change heat transfer (e.g., using heat pipes) may also be used if more compact designs are required. In this study, we will use the most common forced convection of air or water as an example. Assuming that the number of embedded cooling tubes (ECTs) equals N_{ect} and the heat transfer in all ECTs is identical, we have

$$A_{surf} = N_{ect} 2\pi R_{ect} H = C_{As} 2\pi R^2 AR\,. \tag{23}$$

Here, we assume the ECTs are straight and their length inside the tank is equal to the tank height *H*. Thus, the radius of ECTs R_{ect} is obtained as

$$R_{ect} = \frac{C_{As} R}{N_{ect}}. \tag{24}$$

The Nusselt number (Nu) in the ECTs can be estimated via the Dittus–Boelter equation [37, 38]

$$Nu = \frac{2h_{avg} R_{ect}}{k_{coolant}} = 0.023 Re_D^{0.8} Pr^{0.4}. \tag{25}$$

Pr represents the Prandtl number which is respectively 0.71 and 13.6 for air and water at 0 °C. h_{avg} is given by Eq. (19) or (22). Re_D is the Reynolds number defined as

$$Re_D = \frac{2V_{avg} R_{ect}}{\upsilon_{coolant}} \tag{26}$$

where V_{avg} and $\upsilon_{coolant}$ are the coolant average velocity and kinematic viscosity, respectively. Note that other Nu correlations may be used depending on the range of Re_D [38]. Combing Eq. (25) and (26), the total mass flow rate of the coolant is calculated as

$$\dot{m}_{coolant} = N_{ect} \rho_{coolant} \pi R_{ect}^2 V_{avg} = 0.5\pi \rho_{coolant} \upsilon_{coolant} C_{As} R \left(\frac{2h_{avg} R_{ect}}{0.023 Pr^{0.4} k_{coolant}} \right)^{1.25} \tag{27}$$

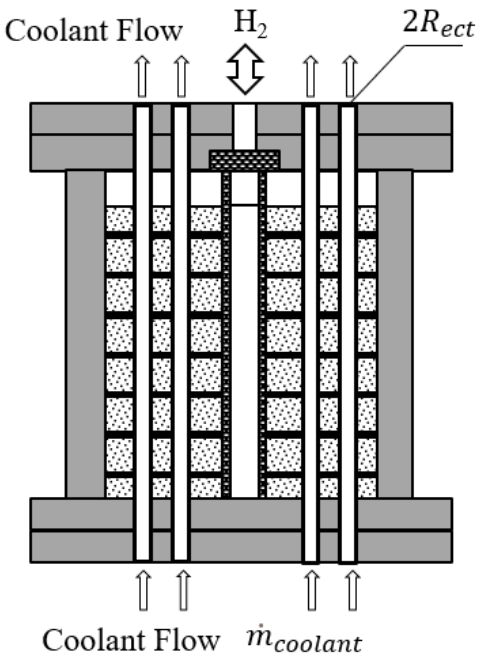

Fig. 7 Internal TMS for solid-state hydrogen storage.

4.2. External TMS

Fig. 8 shows a schematic of the internal TMS using either forced or natural convection. If the external fins are not considered, the problem will be very similar to that in Sec. 4.1,

$$C_{As} = \frac{\pi D_{tank} H}{2\pi R^2 AR} = \frac{D_{tank}}{2R}, \tag{28}$$

where D_{tank} is the outer diameter of the tank. Accordingly, Nu is defined as

$$Nu = \frac{h_{avg} L_c}{k_{coolant}} = f(Re(\dot{m}_{coolant}), Ra, Pr), \tag{29}$$

where L_c is the characteristics length, *f* represents Nu correlation of the external cooling system as a function of Reynolds number (*Re*), Rayleigh number (*Ra*), and *Pr*. Once the *Re* is solved, the mass flow rate can be determined. The external cooling techniques could be external conduction with PCM, external natural convection/thermal radiation, external forced convection generated by a large blower fan/compressor, internal forced convection in a shell-tube heat exchanger, or even boiling heat transfer.

Next, we will consider the case with external fins. Here, we assume a common stacked radial fin configuration. Each fin and the exposed base area have the same heat transfer coefficient h_c. The thermal resistance of the fin and base can be estimated as

$$R_f = \frac{1}{h_c \eta_f A_f} \tag{30}$$

$$R_b = \frac{1}{h_c A_b} \tag{31}$$

where A_f and A_b are the surface area of the fin and base between two consecutive fins and η_f is the thermal efficiency of the fin expressed as [39]

$$\eta_f = \frac{2}{\Phi_1[1 - (\Phi_2/\Phi_1)^2]} \left[\frac{I_1(\Phi_1) - \beta K_1(\Phi_1)}{I_0(\Phi_1) + \beta K_0(\Phi_1)} \right], \tag{32}$$

where I_i and K_i are modified Bessel functioin of the first and second kind respectively with subscript *i* denoting the order of the function. $\beta = I_1(\Phi_2)/K_1(\Phi_2)$ and Φ_1 and Φ_2 are defined by

$$\Phi_1 = \frac{D_{tank}}{2} \sqrt{\frac{2h_c}{k_{fin} t_{fin}}}, \qquad \Phi_2 = \frac{D_{fin}}{2} \sqrt{\frac{2h_c}{k_{fin} t_{fin}}}. \tag{33}$$

D_{fin} are the outer diameter of the fins and t_{fin} is the thickness of the fin. As the heat may transfer through both the fin and base, the total thermal resistance is given by

$$R_{tot,ext} = \frac{1}{N_f \left(\frac{1}{R_f} + \frac{1}{R_b} \right)}, \tag{34}$$

where N_f is the number of fins. Here, we define the equavlent heat transfer coefficient h_e as

$$h_e = \frac{1}{\pi D_{tank} H R_{tot,ext}} = \frac{N_f \left(\frac{1}{R_f} + \frac{1}{R_b} \right)}{\pi D_{tank} H}. \tag{35}$$

The modified total heat transfer coefficient with thermal efficiency is defined as

$$h_{avg} = h_e \eta_s, \tag{36}$$

where η_s is given by

$$\eta_s = \frac{\tanh(\Omega H)}{\Omega H}, \tag{37}$$

and

$$\Omega = \sqrt{\frac{4h_e}{k_{tank} D_{tank}}}. \tag{38}$$

Since Eq. (30)-(38) are implicit equations for D_{fin} and t_{fin}, iteration is required to determine D_{fin} and t_{fin}.

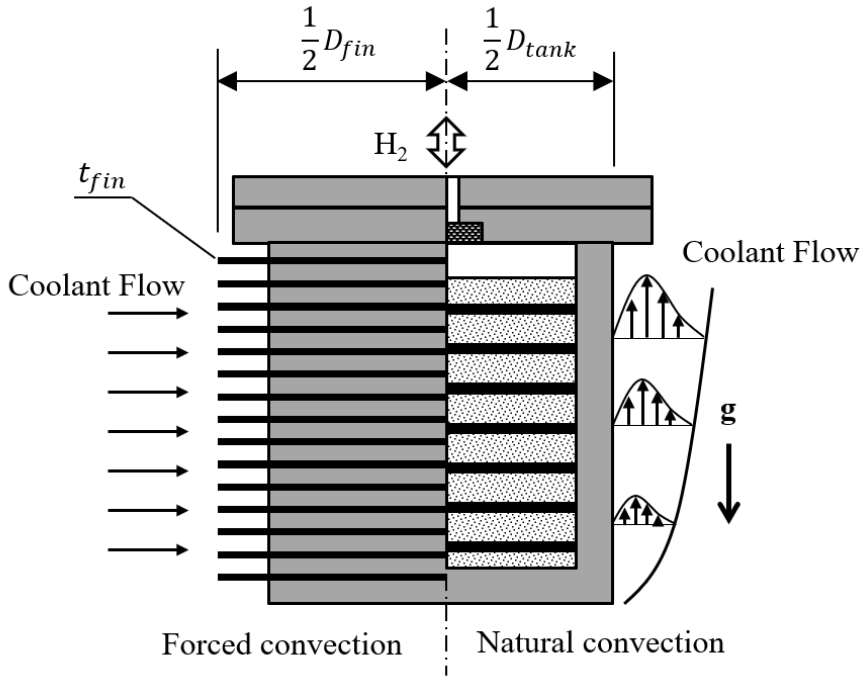

Fig. 8 External TM for solid-state hydrogen storage.

5. Sizing procedures

Fig. 9 shows the procedures for sizing the solid-state TMS. The sizing is based on multi-level models (AM, LPM and/or CFD). First, the storage material, m_g, t_s will be initialized as well as the $C_{wt,e}$ and cost. Then, the tank and internal fins will be first sized using the AM proposed in Sec. 3. Once the tanks are sized, the cooling technique and the size of the corresponding TMS will be determined using the AM in Sec. 4. After the sizing of the tank and TMS are completed, C_{eff} and or cost will be evaluated to see if further iterations are required. If $C_{wt,e}$ and/or cost meets the requirement, more accurate simulations using LPM/CFD will be performed to verify if t_s is converged. If so, the whole sizing ends. Otherwise, the sizing with the AM will be repeated. Note that the sizing may not converge if C_{eff} and cost goals are not reasonable. Furthermore, the CFD simulation will be preferred for the complex bed configurations with internal fins and cooling tubes. Otherwise, for simple bed configuration, LPM is recommended due to its low computational cost compared with CFD. A detailed description of LPM can be found in our previous work [30].

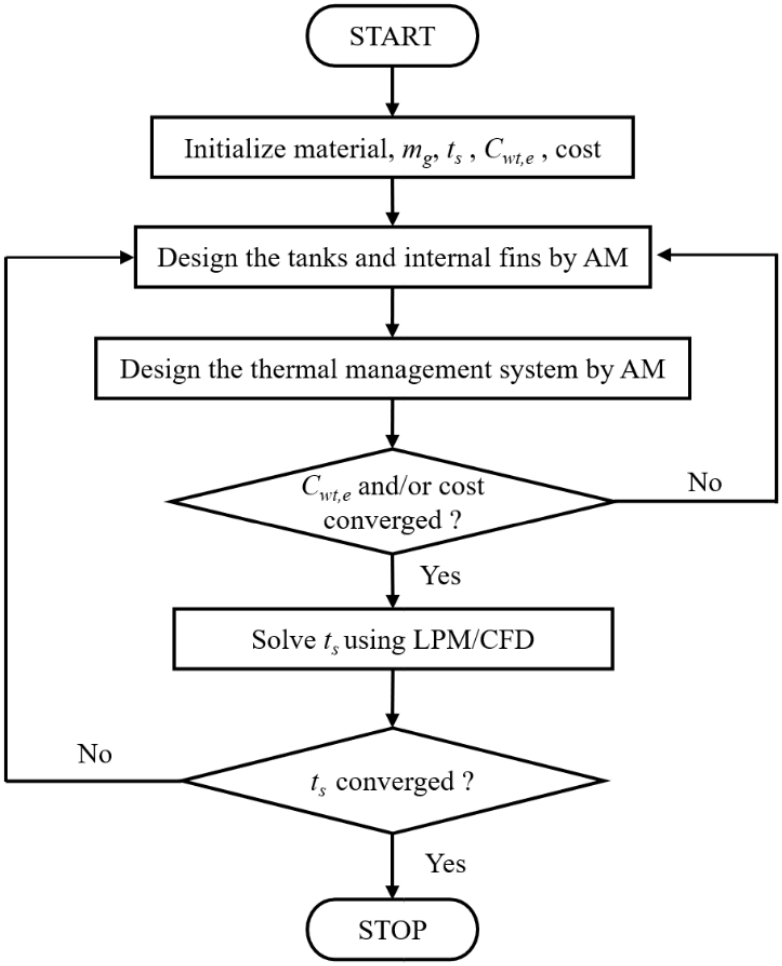

Fig. 9 Procedures for sizing the solid-state hydrogen storage system.

6. Numerical validations

In this section, the proposed AM is validated against the experimental data [7, 8, 23] in Table 2. Here, we assume that the storage material properties, sorption time, and total amount of hydrogen are known and equal to the corresponding experimental results. Also, the volume ratios $C_{ve}, C_{vf}, C_{vt}, C_{vo}$ are the same as those of the experiments. Since the volume ratios are only available in Ref. [7, 8, 23], calculations are conducted for these cases only. Comparisons of the present results by the AM and previous experiment data (baseline case) for the three cases are presented in Table 3. For the tanks, both R and AR are presented. As the detailed information about the fins and cooling tubes or external flows is not presented in the selected papers, we only compute h_{avg} for the TMS.

It is obvious that the predicted results for the tank and TMS agree with those of the experiment except for the h_{avg} in case 1 ($LaNi_5$ reactor). This is because the TMS in the experiment is oversized. As mentioned in Sec. 2, t_s is proportional to the total thermal resistance. If the thermal resistance of the TMS is much smaller than that of the bed, increasing h_{avg} no longer help reduce the sorption time. To further reveal this phenomenon, the LPM simulations are conducted for the same case but with different h_{avg}. Fig. 10 shows the transient variations of ϕ_H for $h_{avg} = 50$, 671, and 1625 W/m^{2}K. The first value is assumed to be an order of magnitude larger than the second value obtained by the AM whereas the third value is from the experiment data. It is observed that there is negligible difference of ϕ_H profiles between the AM predicted value and that of the experiment. However, the ϕ_H profile for the first value differs significantly from the last two values. Apparently,

h_{avg} only influences the adsorption curve when the thermal resistance $R_{th} = 1/(h_{avg}A_{surf})$ of the external cooling system has the same order of magnitude as that of the porous bed.

Table 3 Validations of the proposed AM against the previous experimental data for solid-state H_2 storage systems.

Case no.	Data	Tank		TMS
		R (mm)	AR	h_{avg} (W/m^{2}K)
1	Present	24.3	3.2	671
	Ref. [7]	25	3.2	1625
2	Present	13.7	32.9	1164
	Ref. [8]	13.5	35.2	750-1250
3	Present	49.9	3.0	1192
	Ref. [23]	51.2	3.1	1610-2140

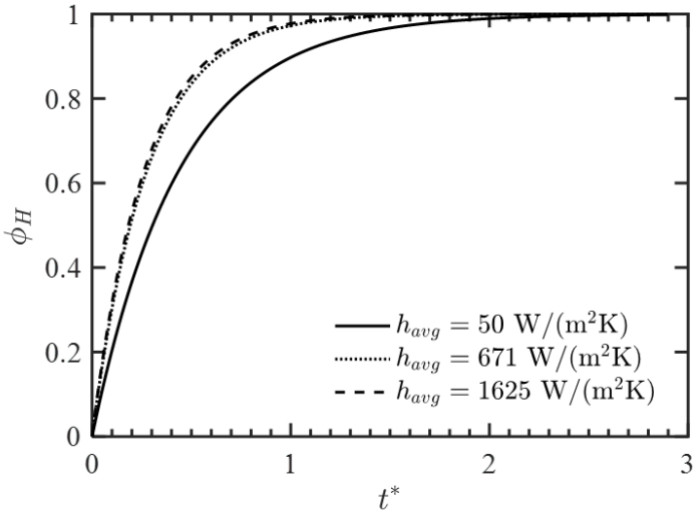

Fig. 10 Comparisons of transient ϕ_H for different h_{avg}.

7. Conclusion

In this study, a multi-level sizing framework is developed to size the solid-state H_2 storage system that consists of the tank and the corresponding TMS. The proposed sizing procedure includes an inner loop and outer loop. Since the AM is used in the inner loop to provide input for more computationally expensive methods such as LPM/CFD, the iterations required for CFD simulations are significantly reduced. Also, the sizing models are directly based on the sorption-time which saves the time for thermal performance optimization. According to the targeted sorption time and effective gravimetric capacity or cost, the sizing models for two broad category TMSs - internal and external- are derived. To validate the sizing model, three cases involving both internal and external cooling techniques are tested, and the results are compared with those of the experiment. Good agreements are attained. Through the validated case, it is also found that t_s is proportional to the total thermal resistance. If the thermal resistance of the TMS is much smaller than that of the bed, increasing h_{avg} no longer helps reduce the sorption time but results in oversized design of the TMS. Finally, as the computational cost for the AM is negligible, it is possible to use the developed method to size large-scale industrial H_2 storage systems with large numbers of cylinder arrays and complex TMSs.

Acknowledgments

This work is sponsored by Mitacs Accelerate grant no. IT16090 and Hydrogen In Motion Inc. (H2M).

References

[1] Abdalla, A. M., Hossain, S., Nisfindy, O. B., Azad, A. T., Dawood, M., & Azad, A. K. (2018). Hydrogen production, storage, transportation and key challenges with applications: A review. Energy Conversion and Management, 165, 602-627.

[2] Yao, J., Zhu, P., Qian, C., Hamidullah, U., Kurko, S., Yang, F., Zhang, Z. and Wu, Z. (2020). Study of an autothermal-equilibrium metal hydride reactor by reaction heat recovery as hydrogen source for the application of fuel cell power system. Energy Conversion and Management, 213, 112864.

[3] Ahmed, A., Seth, S., Purewal, J., Wong-Foy, A. G., Veenstra, M., Matzger, A. J., & Siegel, D. J. (2019). Exceptional hydrogen storage achieved by screening nearly half a million metal-organic frameworks. Nature communications, 10(1), 1568.

[4] Gupta, R. B. (2008). Hydrogen fuel: production, transport, and storage. CRC Press.

[5] Jena, P. (2011). Materials for hydrogen storage: past, present, and future. The Journal of Physical Chemistry Letters, 2(3), 206-211.

[6] Chen, Z., Ma, Z., Zheng, J., Li, X., Akiba, E., & Li, H. (2021). Perspectives and challenges of hydrogen storage in solid-state hydrides. Chinese Journal of Chemical Engineering, 29, 1-12.

[7] Jemni, A., Nasrallah, S. B., & Lamloumi, J. (1999). Experimental and theoretical study of a metal–hydrogen reactor. International Journal of Hydrogen Energy, 24(7), 631-644.

[8] Muthukumar, P., Maiya, M. P., & Murthy, S. S. (2005). Experiments on a metal hydride-based hydrogen storage device. International Journal of Hydrogen Energy, 30(15), 1569-1581.

[9] Phate, A. K., Maiya, M. P., & Murthy, S. S. (2007). Simulation of transient heat and mass transfer during hydrogen sorption in cylindrical metal hydride beds. International Journal of Hydrogen Energy, 32(12), 1969-1981.

[10] Yang, F., Meng, X., Deng, J., Wang, Y., & Zhang, Z. (2008). Identifying heat and mass transfer characteristics of metal hydride reactor during adsorption—Parameter analysis and numerical study. International Journal of Hydrogen Energy, 33(3), 1014-1022.

[11] Yang, F., Meng, X., Deng, J., Wang, Y., & Zhang, Z. (2009). Identifying heat and mass transfer characteristics of metal hydride reactor during adsorption: improved formulation about parameter analysis. International Journal of Hydrogen Energy, 34(4), 1852-1861.

[12] Nam, J., Ko, J., & Ju, H. (2012). Three-dimensional modeling and simulation of hydrogen absorption in metal hydride hydrogen storage vessels. Applied Energy, 89(1), 164-175.

[13] Mellouli, S., Khedher, N. B., Askri, F., Jemni, A., & Nasrallah, S. B. (2015). Numerical analysis of metal hydride tank with phase change material. Applied Thermal Engineering, 90, 674-682.

[14] Lin, X., Zhu, Q., Leng, H., Yang, H., Lyu, T., & Li, Q. (2019). Numerical analysis of the effects of particle radius and porosity on hydrogen absorption performances in metal hydride tank. Applied Energy, 250, 1065-1072.

[15] Manai, M. S., Leturia, M., Pohlmann, C., Oubraham, J., Mottelet, S., Levy, M., & Saleh, K. (2019). Comparative study of different storage bed designs of a solid-state hydrogen tank. Journal of Energy Storage, 26, 101024.

[16] Afzal, M., & Sharma, P. (2021). Design and computational analysis of a metal hydride hydrogen storage system with hexagonal honeycomb based heat transfer enhancements-part A. International Journal of Hydrogen Energy, 46(24), 13116-13130.

[17] Afzal, M., Gupta, N., Mallik, A., Vishnulal, K. S., & Sharma, P. (2021). Experimental analysis of a metal hydride hydrogen storage system with hexagonal honeycomb-based heat transfer enhancements-part B. International Journal of Hydrogen Energy, 46(24), 13131-13141.

[18] Hardy, B. J., & Anton, D. L. (2009). Hierarchical methodology for modeling hydrogen storage systems. Part I: Scoping models. International Journal of Hydrogen Energy, 34(5), 2269-2277.
[19] Hardy, B. J., & Anton, D. L. (2009). Hierarchical methodology for modeling hydrogen storage systems. Part II: Detailed models. International Journal of Hydrogen Energy, 34(7), 2992-3004.
[20] Askri, F., Salah, M. B., Jemni, A., & Nasrallah, S. B. (2009). Optimization of hydrogen storage in metal-hydride tanks. International Journal of Hydrogen Energy, 34(2), 897-905.
[21] Bao, Z., Yang, F., Wu, Z., Cao, X., & Zhang, Z. (2013). Simulation studies on heat and mass transfer in high-temperature magnesium hydride reactors. Applied Energy, 112, 1181-1189.
[22] Singh, A., Maiya, M. P., & Murthy, S. S. (2015). Effects of heat exchanger design on the performance of a solid state hydrogen storage device. International Journal of Hydrogen Energy, 40(31), 9733-9746.
[23] Kumar, A., Raju, N. N., & Muthukumar, P. (2021). Parametric studies on MmNi4. 7Fe0. 3 based reactor with embedded cooling tubes for hydrogen storage and cooling application. Journal of Energy Storage, 35, 102317.
[24] Eisapour, A. H., Naghizadeh, A., Eisapour, M., & Talebizadehsardari, P. (2021). Optimal design of a metal hydride hydrogen storage bed using a helical coil heat exchanger along with a central return tube during the absorption process. International Journal of Hydrogen Energy, 46(27), 14478-14493.
[25] Bai, X. S., Yang, W. W., Tang, X. Y., Yang, F. S., Jiao, Y. H., & Yang, Y. (2021). Optimization of tree-shaped fin structures towards enhanced absorption performance of metal hydride hydrogen storage device: A numerical study. Energy, 220, 119738.
[26] Kikkinides, E. S., Georgiadis, M. C., & Stubos, A. K. (2006). On the optimization of hydrogen storage in metal hydride beds. International Journal of Hydrogen Energy, 31(6), 737-751.
[27] Mellouli, S., Askri, F., Dhaou, H., Jemni, A., & Nasrallah, S. B. (2010). Numerical simulation of heat and mass transfer in metal hydride hydrogen storage tanks for fuel cell vehicles. International Journal of Hydrogen Energy, 35(4), 1693-1705.
[28] Karmakar, A., Mallik, A., Gupta, N., & Sharma, P. (2021). Studies on 10kg alloy mass metal hydride based reactor for hydrogen storage. International Journal of Hydrogen Energy, 46(7), 5495-5506.
[29] Wang, C. S., & Brinkerhoff, J. (2020). Advances in mathematical modeling of hydrogen adsorption and desorption in metal hydride beds with lattice Boltzmann method. International Journal of Hydrogen Energy, 45(56), 32179-32195.
[30] Wang, C. S., & Brinkerhoff, J. (2022). Low-cost lumped parameter modelling of hydrogen storage in solid-state materials. Energy Conversion and Management, 251, 115005.
[31] Lototskyy, M., Tolj, I., Klochko, Y., Davids, M. W., Swanepoel, D., & Linkov, V. (2020). Metal hydride hydrogen storage tank for fuel cell utility vehicles. International Journal of Hydrogen Energy, 45(14), 7958-7967.
[32] Wang, C. S., & Brinkerhoff, J. (2021). Predicting hydrogen adsorption and desorption rates in cylindrical metal hydride beds: Empirical correlations and machine learning. International Journal of Hydrogen Energy, 46(47), 24256-24270.
[33] Wang, C. S., & Brinkerhoff, J. (2021). Is there a general time scale for hydrogen storage with metal hydrides or activated carbon?. International Journal of Hydrogen Energy, 46(21), 12031-12034.
[34] Garrier, S., Chaise, A., de Rango, P., Marty, P., Delhomme, B., Fruchart, D., & Miraglia, S. (2011). MgH2 intermediate scale tank tests under various experimental conditions. International Journal of Hydrogen Energy, 36(16), 9719-9726.
[35] Chaise, A., De Rango, P., Marty, P., & Fruchart, D. (2010). Experimental and numerical study of a magnesium hydride tank. International Journal of Hydrogen Energy, 35(12), 6311-6322.
[36] Kosky, P., Balmer, R., Keat, W., & Wise, G. (2015). Exploring engineering: an introduction to engineering and design. Academic Press.
[37] Liou, T. M., Wang, C. S., & Chan, S. P. (2017). Effect of included angle on turbulent flow and heat transfer in rhombic serpentine heat exchangers. International Journal of Thermal Sciences, 114, 155-171.
[38] Bejan, A. (2013). Convection heat transfer. John Wiley & Sons.
[39] Cengel, Y. A. & Ghajar, A. J. (2015). Heat and mass transfer: fundamentals and applications. McGraw Hill.